13th ewtec 2019 Proceedings of the 13th European Wave and Tidal Energy Conference 1-6 Sept 2019, Naples, Italy

Power capture gains for the WaveSub submerged WEC using active control

Andrew J. Hillis, Craig Whitlam, Annette Brask, John Chapman and Andrew R. Plummer

***Abstract*—An active control strategy is applied to the WaveSub Wave Energy Converter (WEC). The purpose of the control strategy is to maximise power capture across a range of seas whilst operating within physical system constraints. WaveSub uses four rotational PTOs attached to drums which are driven by taut tethers connected to a float. The full scale WEC has been modelled in the WEC-Sim environment using a fixed passive damping system for the PTOs, which was optimally tuned for individual sea-states to provide a performance benchmark. An active control system utilising the simple and effective method with a Linear Quadratic Regulator velocity tracking loop is developed. A range of sea states is applied and the performance of the active and passive systems compared. Power gains of 13% to 86% are observed across a wide range of irregular sea states compared to the optimally tuned passive system. This approach shows promise to provide a substantial increase in power capture for a minimal additional device cost and therefore a significant improvement in cost of energy would likely result.**

***Keywords*–Active control, submerged Wave Energy Converter, power take off**

I. Introduction

WaveSub is under development by Marine Power Systems Ltd (MPS). It is a submerged point absorber with a unique multi-tether configuration and variable geometry which can be tuned to the prevailing sea state. A float moves with the waves and reacts against a moored base. The tethers pull on rotational drums which are attached to a PTO. An illustration of a full scale multi-float concept is shown in Figure 1.

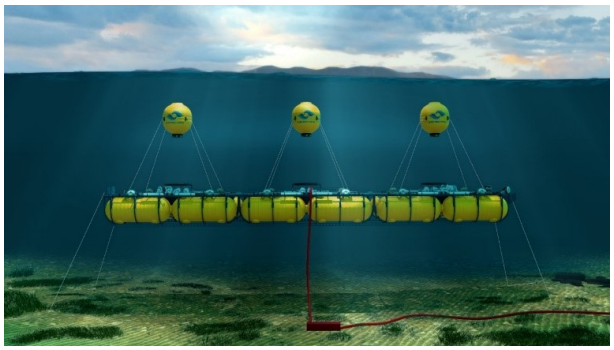

Fig. 1. Illustration of full scale multi-float WaveSub concept

Paper #1313. Grid integration, power take-off and control. This research was supported in part by the Wave Energy Scotland Controls competition. A.J. Hillis and A.R. Plummer are with the Department of Mechanical Engineering, University of Bath, Bath BA27AY, UK (e-mail: a.j.hillis@bath.ac.uk, a.r.plummer@bath.ac.uk). J. Chapman, C. Whitlam and A. Brask are with WaveSub developers Marine Power Systems Ltd, Ethos Building, Kings Road, Swansea, SA1 8AS (e-mail: contact@marinepowersystems.co.uk).

This study uses a single section of this device, comprising a single float with four taut tethers connected to individual drums and rotational PTOs. The block diagram of the complete system is shown in Figure 2.

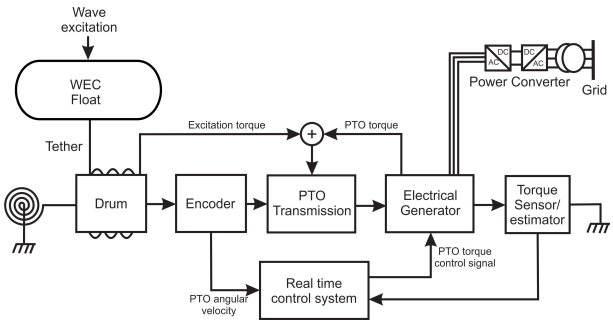

Fig. 2. Block diagram representation of WEC/PTO systems

Active control strategies generally aim to achieve efficient power capture by keeping the velocity of the primary converter in phase with the wave excitation force. This may be achieved in an ideal manner through complex-conjugate control, for example see [1]. Practical implementation of complex-conjugate control is difficult as it is non-causal and can result in very large forces and motions of the device which could violate physical constraints. Alternative sub-optimal approaches have been proposed, for example latching and declutching control [2][3][4], which engage or disengage the PTO at a specified time. The disadvantage of these strategies is that they can result in large forces being transmitted to the WEC structure and PTO. Model Predictive Control (MPC) strategies have also been applied, see for example [5][6][7]. These have the advantage that physical constraints can be incorporated, but the optimisation problem may be computationally intensive for a realistic nonlinear WEC and PTO making real-time implementation problematic [8]. Additionally, MPC depends on accurate plant models and requires prediction of the wave excitation which increases uncertainty and potentially reduces robustness.

An alternative solution is the Simple and Effective controller proposed in [9], whereby a computed velocity reference signal is designed to keep the WEC velocity in phase with the wave excitation while also considering physical constraints such as position limits. Velocity tracking is achieved by a feedback control loop and many architectures are suitable for this purpose. In [10] a State Feedback with Integral Action (SFCIA) controller is used and good performance was found when applied to an idealised model of a nonlinear OSWEC. In [11] an adaptive strategy is applied to the same WEC to improve performance with a highly nonlinear hydraulic PTO. In [12] the Simple and Effective strategy is applied

to a submerged WEC with three taut tethers using an Internal Model Control loop for velocity tracking and good performance is reported. Here the Simple and Effective strategy is applied to a full scale WEC-Sim model of the WaveSub submerged WEC. A Linear Quadratic Regulator state feedback loop is used for velocity tracking, including full modal coupling. Performance is compared to an optimally tuned passively controlled system in a wide range of irregular sea states.

Descriptions of the WEC models are provided in sections II and III. The control strategy is described in section IV and integration with WEC-Sim is discussed in section V. Simulation results comparing the passive benchmark system performance against the actively controlled system under realistic conditions are provided in section VI. Conclusions are provided in section VII.

II. Baseline WEC Simulation

A. Model Description

A 1:25 scale WEC-Sim model of a single float system using four PTO tethers and a taut mooring system has been validated against experimental data from wave tank testing. A full-scale WEC-Sim model has been extrapolated from the 1:25 scale model and is the subject of this study. The optimum passive spring-damper combinations have been established across the full range of operational irregular sea conditions and this system is used as a benchmark for performance comparison against an actively controlled PTO system. Figure 3 shows an image of the simplified geometry used for simulation in the WEC-Sim package. The dimensions are given in table I.

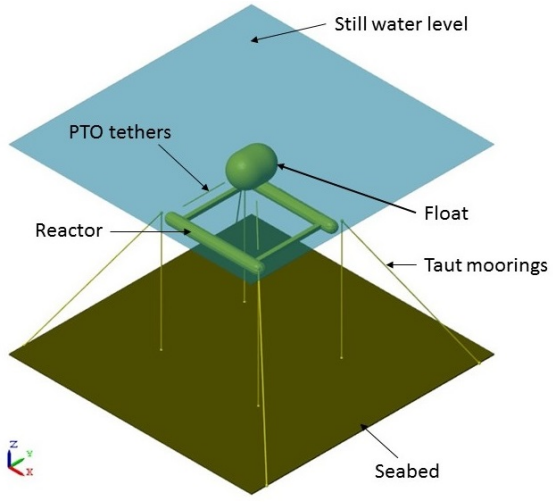

Fig. 3. Simplified geometry and mooring in WEC-Sim

The float and reactor are connected with four taut PTO tether lines, each modelled as a translational PTO actuation force incorporating a spring stiffness and damping force, a universal joint and gimbal. All motions and forces are available for use by the control strategy within this model and the control force applied to each PTO is incorporated by adding to the external preload force on each PTO. The damping force is used only for the benchmark passive optimally tuned system and is set to zero for active control. Irregular waves are applied in the x-direction.

TABLE I
Dimensions of the geometry of the full scale WEC-Sim model

Properties	Value	Unit
Float diameter	12	m
Float cylinder length	4.75	m
Reactor length	51.55	m
Reactor width	50	m
Reactor height	4.85	m

Results using a Pierson-Moskovitz (PM) spectrum with significant wave height $H_s = 3\text{m}$ and energy period $T_e = 10\text{s}$ (see Figure 4) are presented in detail, giving insight into the internal signals and processes occurring within the passive and active control systems. This sea state represents a typical sea state for which the device is sized. A wide range of PM spectra with $H_s = 0.5 - 6.5\text{m}$ and $T_e = 6 - 16\text{s}$ are latterly used for mean power capture comparison.

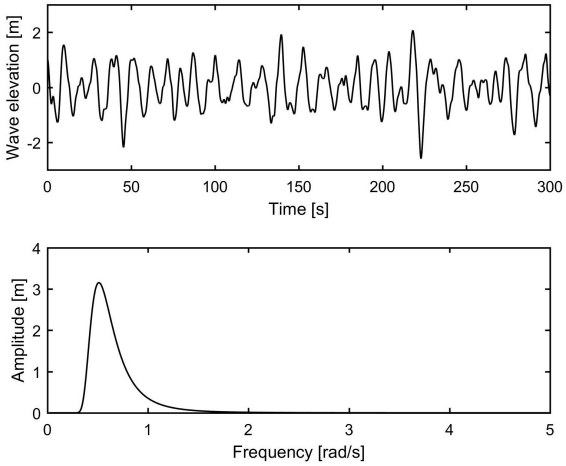

Fig. 4. Wave elevation and spectrum for irregular waves (Pierson-Moskovitz with $H_s = 3\text{m}$ $T_e = 10\text{s}$)

B. Forces acting on the float body

The governing equation of motion for the float body is:

$$\mathbf{M}\ddot{\mathbf{x}} = \mathbf{F}_h(t) + \mathbf{F}_m(t) \tag{1}$$

where $\mathbf{M}$ is the float mass matrix, $\ddot{\mathbf{x}}$ is the float acceleration vector, $\mathbf{F}_h(t)$ is the total hydrodynamic force vector and $\mathbf{F}_m(t)$ is the mechanical force vector of the PTO. Assuming linear wave theory, the hydrodynamic force can be decomposed as follows:

$$\mathbf{F}_h(t) = \mathbf{F}_e(t) + \mathbf{F}_r(t) + \mathbf{F}_{hs}(t) + \mathbf{F}_v(t) \tag{2}$$

where $\mathbf{F}_e(t)$, is the excitation force produced by an incident wave on an otherwise fixed body, $\mathbf{F}_r(t)$ is the radiation force which is produced by an oscillating body creating waves on an otherwise still sea, and $\mathbf{F}_{hs}(t)$ is the hydrostatic restoring force. $\mathbf{F}_v(t)$ is a nonlinear viscous damping term which is commonly neglected.

$\mathbf{F}_{hs}(t)$ is constant as the float is fully submerged. In the heave direction it is given by

$$F_{hs}(t) = -\rho g V \tag{3}$$

where ρ is the water density, g is the acceleration due to gravity and V is the float volume.

The radiation force in the time domain is given by [13]

$$\mathbf{F}_r(t) = -\mathbf{A}_\infty \ddot{\mathbf{x}} - \int_0^t \mathbf{K}_r(t-\tau)\dot{\mathbf{x}}(\tau)d\tau \tag{4}$$

where $\mathbf{A}_\infty$ is the infinite frequency added mass matrix, $\mathbf{K}_r$ is the radiation impulse function and $\mathbf{x} \in R^{6\times 1}$ is the state vector given by

$$\mathbf{x} = [x\ y\ z\ \theta_x\ \theta_y\ \theta_z]^T \tag{5}$$

The excitation and radiation forces are calculated using hydrodynamic coefficients computed by the NEMOH BEM solver [14].

C. Optimal tuning of PTO stiffness and damping

The passively damped system uses a fixed damping coefficient on each PTO. The optimal damping co-efficient is dependent on the peak period of the wave spectrum applied. For each sea state tested the passive damping co-efficient and spring stiffness were optimally tuned. The optimal parameters are shown in Figure 5.

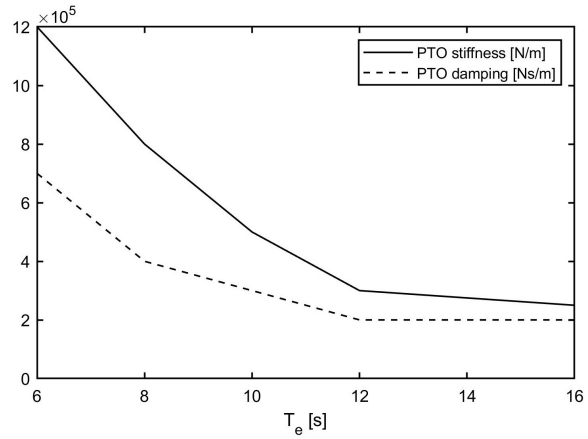

Fig. 5. Optimal stiffness and damping curves for passive WEC

As such the passive system benchmark performance represents the highest possible captured power with a fixed damping coefficient in a given sea state. In practice to achieve this, the damping coefficient would need to vary as the incident sea state varies resulting in a slow-tuning control strategy. Performance decays sharply if the damping is poorly tuned and tuning in operation would depend upon good estimation of the peak energy period of the incident sea-state. This is not always possible due to long data lengths required, and the lack of a defined peak or double peaks in some seas.

III. Linearised dynamic system model

For model-based control system design, a linearised approximation to the WEC and PTO systems is typically required. Assuming the reactor is fixed (which is acceptable with the taut mooring system) we can use the approach of [15] and [12]. The plant dynamics may be represented by the state-space system given by

$$\begin{gathered}\dot{\mathbf{x}}' = \left[\begin{array}{c}\dot{\mathbf{x}}\\ \ddot{\mathbf{x}}\\ \hline \dot{\mathbf{p}}_r\end{array}\right] = \mathbf{A}\mathbf{x}' + \mathbf{B}(\mathbf{F}_e + \mathbf{u}) \\ y = \mathbf{C}\mathbf{x}'\end{gathered} \tag{6}$$

where $\mathbf{u}$ is the 6DOF control force vector and the state vector is given by $[\mathbf{x}\ \ \dot{\mathbf{x}}]^T$. The state vector is augmented with the auxiliary states $\mathbf{p}_r$ relating to a 4^{th} order State-Space approximation $\mathbf{G}_r$ of the radiation impulse response functions described by

$$\begin{gathered}\dot{\mathbf{p}}_r = \mathbf{A}_r\mathbf{p}_r + \mathbf{B}_r\dot{\mathbf{x}} \\ \int_0^t \mathbf{K}_r(t-\tau)\dot{\mathbf{x}}(\tau)d\tau \approx \mathbf{C}_r\mathbf{p}_r + \mathbf{D}_r\dot{\mathbf{x}}\end{gathered} \tag{7}$$

where the matrices $\{\mathbf{A}_r, \mathbf{B}_r, \mathbf{C}_r, \mathbf{D}_r\}$ describing $\mathbf{G}_r$ are computed in the BEMIO code supplied with WEC-Sim. Including all 36 modes in the state-space model results in 144 states.

The augmented plant and output matrices are obtained from linearising the WEC system about its nominal resting position. These are given by equations 8-10 where $\mathbf{A}_\infty$ is obtained from the BEM solution, $\mathbf{K}_0$ is the linearised stiffness matrix (see [15]) and $\mathbf{B}_v$ is a linear viscous damping matrix empirically tuned to give a reasonable match to experimental data. The state-space model order can be reduced by obtaining a balanced state-space realization and eliminating states with negligible contribution to the system response. Using this approach the total number of states can be reduced to 44, resulting in a model suitable for control system design.

Figure 6 shows the surge, heave and pitch float velocities under controlled conditions. Results are shown for three irregular sea states with the same peak period and increasing significant wave heights. The reduced order linearised model shows good agreement, with accuracy reducing with increased wave height. This is to be expected as the model is linearised about its resting position and accuracy will degrade as the PTO tether angles change for large motions.

$$\mathbf{A} = \left[\begin{array}{cc|c} \mathbf{0}^{6\times 6} & \mathbf{I}^{6\times 6} & \mathbf{0}^{6\times 144} \\ -(\mathbf{M}+\mathbf{A}_\infty)^{-1}\mathbf{K}_0 & -(\mathbf{M}+\mathbf{A}_\infty)^{-1}(\mathbf{B}_v+\mathbf{D}_r) & -(\mathbf{M}+\mathbf{A}_\infty)^{-1}\mathbf{C}_r \\ \hline \mathbf{0}^{144\times 6} & \mathbf{B}_r & \mathbf{A}_r \end{array}\right] \tag{8}$$

$$\mathbf{B} = \left[\begin{array}{c} \mathbf{0}^{6\times 6} \\ (\mathbf{M}+\mathbf{A}_\infty)^{-1} \\ \hline \mathbf{0}^{144\times 6} \end{array}\right] \tag{9}$$

$$\mathbf{C} = \left[\begin{array}{cc|c} \mathbf{0}^{6\times 6} & \mathbf{I}^{6\times 6} & \mathbf{0}^{6\times 144} \end{array}\right] \tag{10}$$

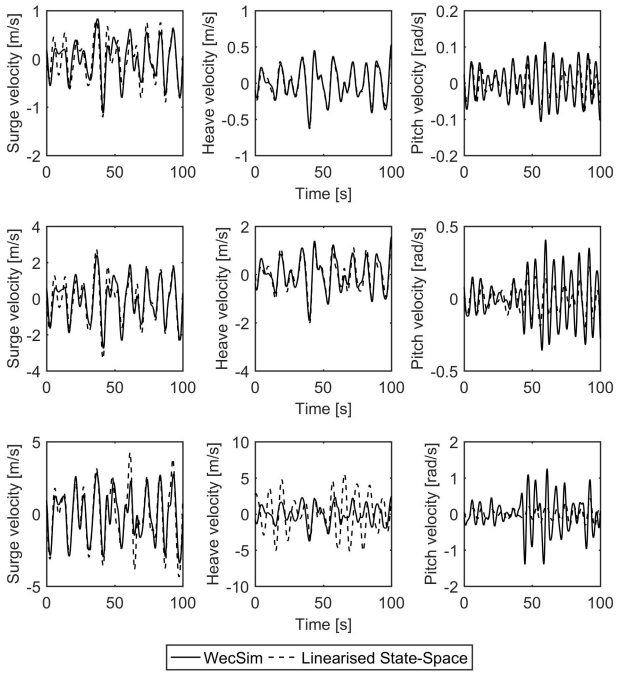

Fig. 6. Surge, heave and pitch float velocities under controlled conditions. Results shown for three sea states with $T_e = 10s$ and $H_s = 1m$ (TOP), $H_s = 3m$ (MIDDLE), $H_s = 6m$ (BOTTOM)

IV. Active control methodology

Here we adopt the Simple and Effective strategy proposed in [9], whereby a velocity reference trajectory is evolved based upon the wave excitation force and knowledge of the plant dynamics and constraints. The overall control strategy is illustrated in Figure 7.

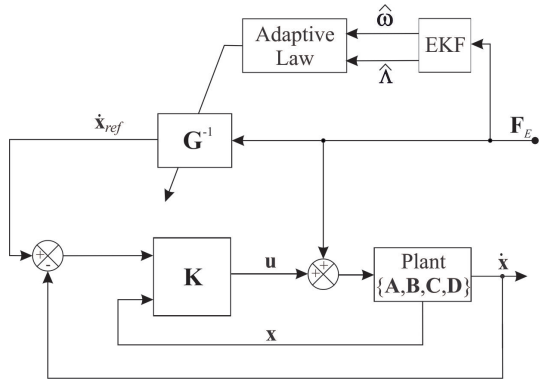

Fig. 7. Illustration of Simple and Effective control strategy with LQR velocity tracking (adapted from [9])

The vector of Cartesian velocity reference signals is given by

$$\dot{\mathbf{x}}_{ref}(t) = \mathbf{G}^{-1}(t)\mathbf{F}_E(t) = 0.5(|\mathbf{G}_r(\hat{\omega})| + \mathbf{B}_v)^{-1}\mathbf{F}_E(t) \quad (11)$$

where $|\mathbf{G}_r(\hat{\omega})|^{-1} \in R^{6\times 6}$ is the inverse of a time varying matrix of the instantaneous amplitudes of the 4^{th} order state space radiation damping model at the current estimated dominant excitation frequency $\hat{\omega}$. $\mathbf{F}_E(t)$ is assumed to be a narrow band harmonic process of the form [9]

$$\mathbf{F}_E(t) = \mathbf{\Lambda}\cos(\boldsymbol{\omega}t + \boldsymbol{\phi}) \quad (12)$$

It is necessary to estimate the dominant amplitude $\hat{\Lambda}$ and frequency $\hat{\omega}$ of the excitation force for each DOF. This is achieved using an extended Kalman Filter (EKF) as described in section V-B and as mentioned in [9]. Linear position constraints are required to avoid impacts between the float and reactor. Position constraints are readily incorporated as a velocity constraint under the narrow band assumption and the velocity reference gain has an upper bound given by $\bar{\mathbf{G}}^{-1} = \hat{\omega}.\bar{\mathbf{x}}./\hat{\Lambda}$ where $\{.\}$ denotes elementwise multiplication or division and $\{^{-}\}$ is the maximum permissible value of a quantity. Thus a real-time variable gain on the velocity reference may be expressed as

$$\mathbf{G}^{-1}(t) = \begin{Bmatrix} 0.5(|\mathbf{G}_r| + \mathbf{B}_v)^{-1} : \bar{\mathbf{G}}^{-1} \geq 0.5(|\mathbf{G}_r| + \mathbf{B}_v)^{-1} \\ \bar{\mathbf{G}}^{-1} \qquad : \qquad \text{otherwise} \end{Bmatrix} \quad (13)$$

In this study the waves are unidirectional in the x-direction, so only surge and heave motion need to be controlled to prescribed trajectories.

Tracking of the velocity reference is achieved using a Linear Quadratic Regulator (LQR) state feedback controller under the assumption all states may be measured or accurately estimated. **K** is obtained from LQR optimisation to minimise the cost function

$$J(u) = \int_0^\infty \left(\mathbf{x}_e^T\mathbf{Q}\mathbf{x}_e + \mathbf{u}^T\mathbf{R}\mathbf{u}\right) dt \quad (14)$$

where $\mathbf{x}_e$ is the error state trajectory given by

$$\mathbf{x}_e = \begin{bmatrix} \mathbf{0}^{6\times 1} \\ \dot{\mathbf{x}}_{ref} \end{bmatrix} - \begin{bmatrix} \mathbf{x} \\ \dot{\mathbf{x}} \end{bmatrix} \quad (15)$$

The resulting state feedback gain is

$$\mathbf{K} = \mathbf{R}^{-1}\mathbf{B}^T\mathbf{S} \quad (16)$$

where **S** is the solution to the algebraic Riccati equation

$$\mathbf{A}^T\mathbf{S} + \mathbf{S}\mathbf{A} - \mathbf{S}\mathbf{B}\mathbf{R}^{-1}\mathbf{B}^T\mathbf{S} + \mathbf{Q} = 0 \quad (17)$$

and the weighting matrices are designed to balance control effort against tracking performance. Similar to [16], for **Q** we choose

$$\mathbf{Q} = \mathbf{C}^T\bar{\mathbf{Q}}\mathbf{C} \quad (18)$$

where $\bar{\mathbf{Q}} \in R^{6\times 6}$ is the auxiliary output error weighting matrix given by

$$\bar{\mathbf{Q}} = \frac{\bar{T}}{\bar{v}^2}\begin{bmatrix} |diag([\mathbf{e}_{si}])| & \mathbf{0}^{3\times 3} \\ \mathbf{0}^{3\times 3} & r.|diag(\mathbf{F}_i \times \mathbf{e}_{si})| \end{bmatrix} \quad (19)$$

where T and v are the PTO tether tension and velocity respectively, and r is the radius of the float. With reference to Figure 8, $\mathbf{F}_i$ is the the float connection point coordinate vector relative to the float centre of gravity and $\mathbf{e}_{si}$ is the unit vector along the direction of the i^{th} PTO tether in the nominal WEC position. As the system has $x-y$ symmetry it does not matter which line is used.

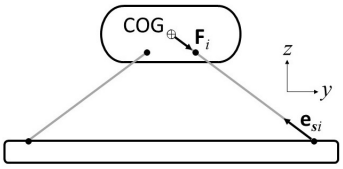

Fig. 8. Illustration of WEC kinematics

The control effort weighting is chosen as

$$\mathbf{R} = \frac{1}{\overline{T}} diag\left[\rho_1 \ \rho_2 \ ... \ \rho_6\right] \tag{20}$$

with ρ_i chosen appropriately to weight control effort in each DOF and achieve good tracking performance.

The control law in Cartesian coordinates is given as

$$\mathbf{u} = -\mathbf{K}\mathbf{x}_e \tag{21}$$

Distribution of $\mathbf{u}(t)$ to the four PTOs is achieved according to

$$\mathbf{u}_{PTO} = \mathbf{J}_0^T \mathbf{u} \tag{22}$$

where $\mathbf{J}_0^{-1}$ is the inverse kinematic Jacobian matrix given by [17]

$$\mathbf{J}_0^{-1} = \begin{bmatrix} \mathbf{e}_{s1}^T & \left(\mathbf{F}_1 \times \mathbf{e}_{s1}\right)^T \\ \vdots & \vdots \\ \mathbf{e}_{s4}^T & \left(\mathbf{F}_4 \times \mathbf{e}_{s4}\right)^T \end{bmatrix} \tag{23}$$

V. Integration with WEC-Sim

The active control algorithm was integrated with the WEC-Sim model to assess any performance benefits over the optimal passive system. The intention was to implement the control in as realistic a manner as possible. Tether tensions and PTO drum rotational velocity and position are assumed measurable. Float motion in Cartesian co-ordinates and the wave excitation force are estimated as described in the following sections.

A. Estimation of float motion

The float motion and position must be measured or estimated for state feedback control. The desirable solution is to measure PTO drum rotational velocity and position using encoders on the drum shafts. Transforming in this direction results in an underdetermined system as there are four equations and six unknowns, therefore it is difficult to estimate the Cartesian velocities accurately. A good partial estimate can be achieved for some degrees of freedom by using a weighted pseudo-inverse, such that the Cartesian velocities are estimated by:

$$\dot{\mathbf{x}} = \mathbf{W}\left(\mathbf{J}_0^{-1}\mathbf{W}^T\right)^{\dagger} \dot{\mathbf{l}} \tag{24}$$

where (†) represents the pseudo-inverse, $\dot{\mathbf{l}}$ is the vector of measured PTO tether velocities and $\mathbf{W}$ is the diagonal weighting matrix. In this case the sway, yaw and roll modes are weighted low to force the accurate estimation of surge and heave velocities. This is acceptable here as Wec-Sim can only apply planar waves, so there is negligible motion induced in the sway, roll and yaw modes. This would also be acceptable in a real deployment in areas with directional waves and the WEC is oriented correctly, as is the current intention of MPS. Pitch velocity is uncontrollable as the PTO tethers point to the float COG in the nominal position. If a higher degree of control were required, it would be possible to mount a battery powered inertial measurement unit (IMU) on the float to directly measure velocities in all six DOFs, in which case this transformation from PTO line space would not be required. Figure 9 shows the true and estimated float motions for surge and heave, very good agreement is observed.

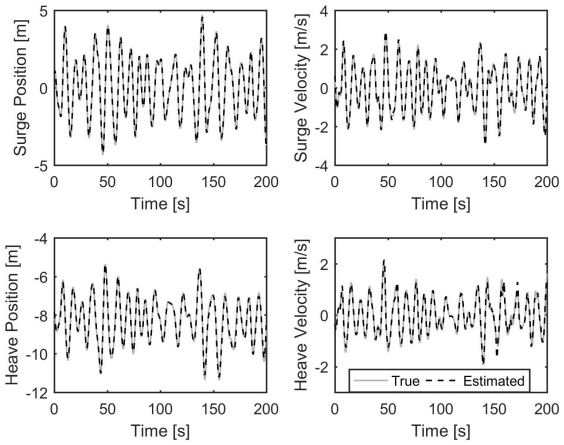

Fig. 9. Estimation of float position and velocity in irregular waves (Pierson-Moskovitz with $H_s = 3$m $T_e = 10$s

B. Estimation of wave excitation force

The wave excitation or disturbance force is not measurable, but is required for the proposed control strategy. In order to estimate the disturbance force it is required to know the dynamics of the float body and all other forces acting upon it, as well as estimates or measurements of the float motion. Float motion and all forces other than the excitation force are readily measured or estimated as previously described. It this then straightforward to implement a dynamic observer to estimate the wave excitation force. Figure 10 shows good estimation of the excitation force for surge and heave directions using such an observer.

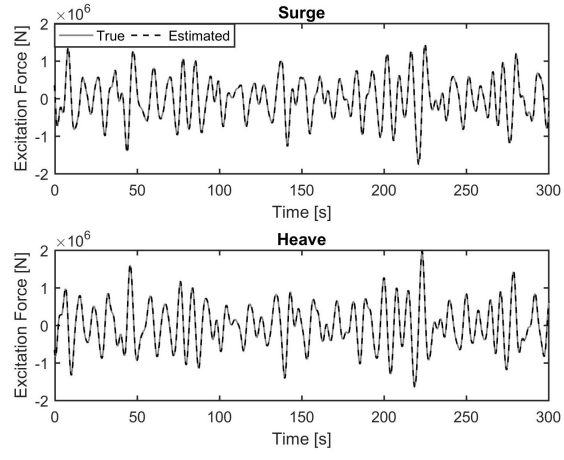

Fig. 10. Estimation of wave excitation force in surge and heave directions in irregular waves (Pierson-Moskovitz with $H_s = 3$m $T_e = 10$s

Once the estimated excitation force has been obtained it is required to estimate its instantaneous amplitude and frequency for use in generating the velocity reference signal for control. This is achieved using an Extended Kalman Filter (EKF). Under the narrow-band assumption, the excitation force is modelled as a single sinusoidal signal with variable amplitude and frequency. The EKF is formulated such that the amplitude and frequency are states to be estimated. Figure 11 shows the amplitude and frequency estimation of an observed signal for the wave excitation force in surge and heave for irregular waves obtained from the Wec-Sim simulation.

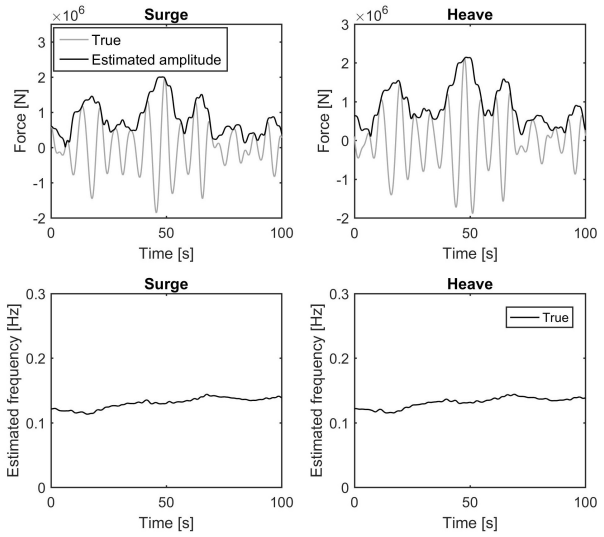

Fig. 11. EKF wave force amplitude and frequency estimation

VI. Simulation results

For detailed insight into the actively controlled system performance, the irregular sea-state of Figure 4 was imposed upon the full nonlinear WEC-Sim model. Figure 12 shows the surge and heave reference and measured float velocities. An achievable velocity reference signal has been generated and the active control strategy is clearly seen to provide good tracking.

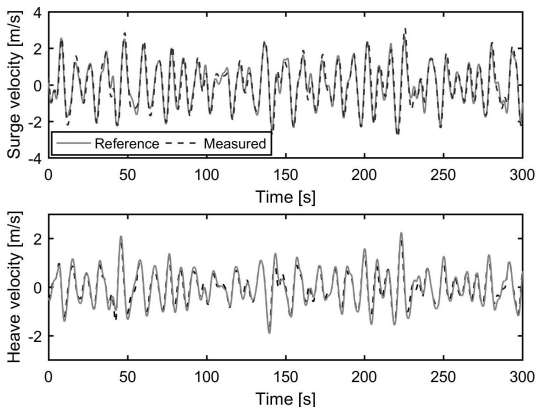

Fig. 12. Surge and heave reference and measured float velocities under controlled conditions (sea state $H_s = 3m$, $T_e = 10s$) for full WEC-Sim model

Displacement limits from nominal of $\pm$5m in surge and $\pm$3m in heave were imposed. Figure 13 shows that the displacement limits are largely adhered to. These limits are imposed in a soft manner, so a factor of safety can be applied if it is critical that they are not exceeded. Though it is not controlled, the pitch motion is included for completeness.

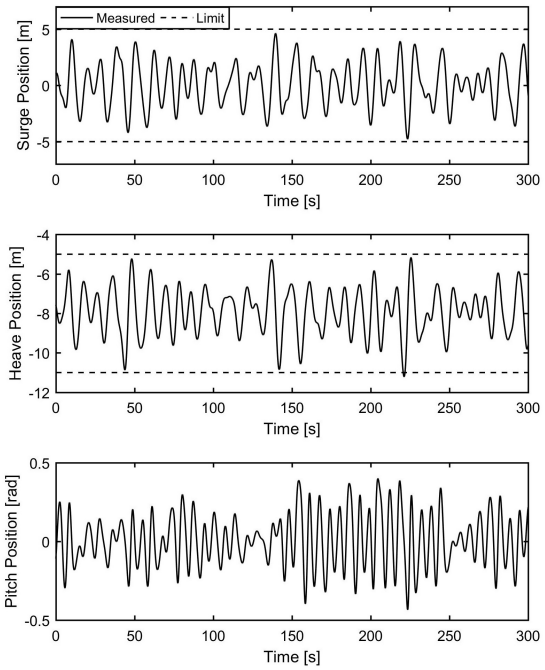

Fig. 13. Surge, heave and pitch float positions under controlled conditions (sea state $H_s = 3m$, $T_e = 10s$) for full WEC-Sim model

Figure 14 shows the mean and peak PTO tether tension for the passive and actively controlled systems.

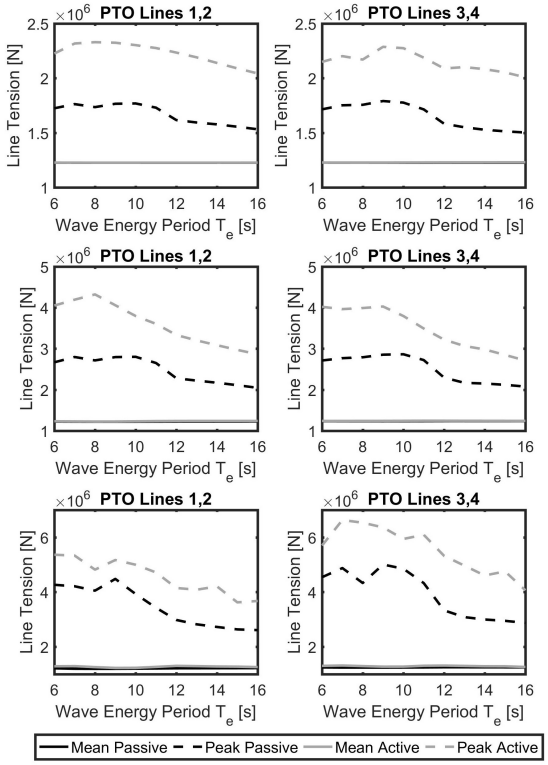

Fig. 14. Mean and peak PTO tether tension for passive and active control for full WEC-Sim model. Results shown for three sea states with $T_e = 10s$ and $H_s = 1m$ (TOP), $H_s = 3m$ (MIDDLE), $H_s = 6m$ (BOTTOM)

The peak tether tensions are larger for the actively controlled system as expected, being generally 50% higher than the passive system peak values.

Figure 15 shows the applied PTO control forces and the resulting PTO tether tensions which are the combination of the control force, pre-tension and spring force. The tether tensions are seen to become positive occasionally. In larger seas this effect would be more prevalent. In reality this is not possible and the PTO tethers would become slack, causing issues for controllability and potentially resulting in snatching loads being transmitted. This is an issue which needs to be resolved in future work. The pre-tension could be increased for larger sea states, or the control methodology modified to prevent this from occurring.

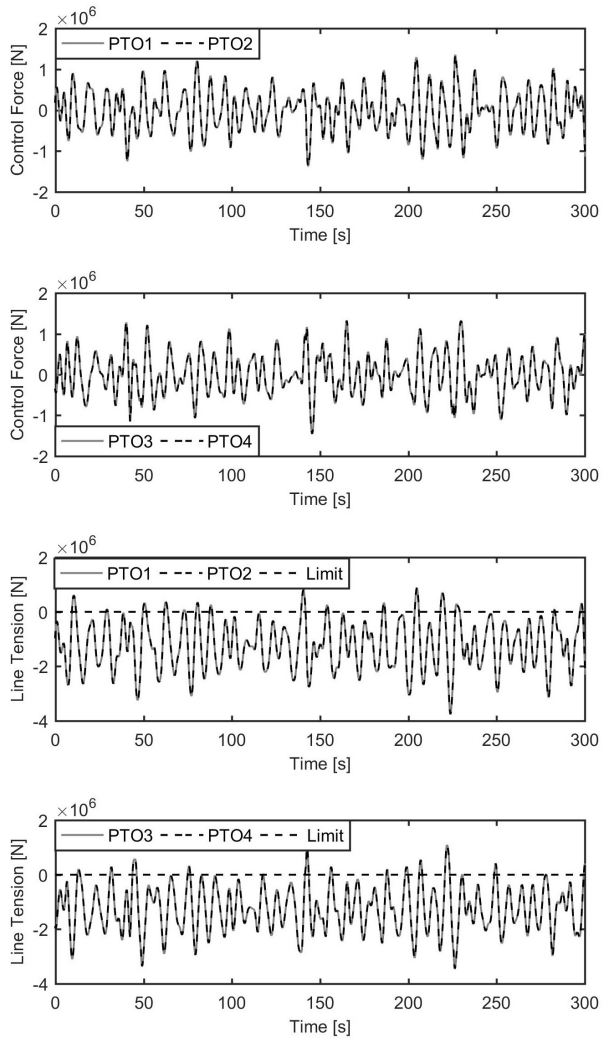

Fig. 15. Control forces and tether tensions under controlled conditions (sea state $H_s = 3m$, $T_e = 10s$) for full WEC-Sim model

Figure 16 shows the instantaneous and mean generated power for the passive and actively controlled systems. Increased power is clearly seen for the actively controlled system, though it would also require more smoothing than the passively controlled output. The reactive power component is clearly seen as negative power when the controller commands a motoring action from the PTOs. This is not always possible or desirable due to the increased cost and complexity of components. Two-quadrant operation may be favourable in many situations, and operates as a restriction of uni-directional power flow i.e. the generator can only generate in both directions, motoring is not permitted. This restriction may be readily incorporated to the active control strategy. This will impact on system performance, but the benefits come in the form of reduced cost and complexity of the components required to achieve the PTO power generation.

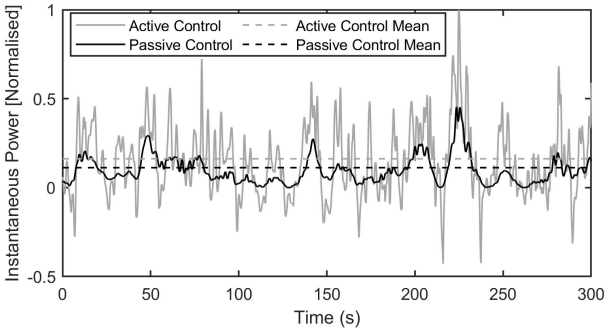

Fig. 16. Instantaneous power under controlled conditions (sea state $H_s = 3m$, $T_e = 10s$) for full WEC-Sim model

Figure 17 shows the percentage increase in mean power generation achieved by the actively controlled system over 700s of simulation with the full nonlinear WEC-Sim model. The results are shown for irregular PM spectra with $H_s = 0.5 - 6.5\text{m}$ and $T_e = 6 - 16\text{s}$. Power gains of 13% to 86% are observed across a wide range of irregular sea states compared to the passive system.

0.5	44	53	60	69	74	75	66	68	72	78	86
1	43	51	56	64	68	68	60	61	64	69	75
1.5	42	49	53	58	62	62	55	56	58	61	66
2	40	46	49	53	57	57	51	50	52	56	61
2.5	38	43	45	49	52	52	46	46	48	52	56
3	36	40	41	44	47	47	41	42	44	47	51
3.5	33	37	38	40	41	42	38	38	39	43	47
4	30	34	35	35	37	36	34	34	35	37	42
4.5	27	31	31	33	34	33	32	30	31	33	37
5	25	27	27	30	32	25	26	20	28	30	33
5.5	22	23	24	27	23	24	23	24	21	27	31
6	19	20	20	22	21	21	18	18	21	20	27
6.5	17	18	18	16	20	21	13	15	17	14	25
Hs [m]/Te [s]	**6**	**7**	**8**	**9**	**10**	**11**	**12**	**13**	**14**	**15**	**16**

Fig. 17. Power matrix showing power percentage increase compared to optimal passive benchmark system for a range of irregular seas with peak period T_e and significant wave height H_s

It is important to note that all performance gains reported here are relative to the optimally tuned passive system. This means that the passive system damping coefficient was individually tailored to a given seastate. The power capture of the passive system is very sensitive to this damping coefficient, and large power reductions would be seen for a detuned system. The passive system damping coefficient would need to be adjusted in service based upon the peak period of the seastate estimated from measurement. This process is subject to errors, particularly for seastates with multiple peaks. Therefore the performance benefits of the actively controlled system would be expected to be greater in a deployed system, as

it is not reliant on such measurements and the inherent uncertainty associated with them.

VII. Conclusions

The Marine Power Systems WaveSub WEC has been modelled in the WEC-Sim environment and an optimally tuned passively damped configuration has been used as a performance benchmark. An active control strategy based upon the Simple and Effective method is implemented. A velocity reference vector is calculated from the estimated wave excitation force, taking into account displacement constraints. Velocity tracking is achieved using a coupled Linear Quadratic Regulator state feedback loop with the state and control weighting matrices tuned to balance tracking performance with control effort. The passive and actively controlled systems were tested in WEC-Sim with a range of PM irregular sea states. Good performance is observed for the actively controlled system and mean power increases of between 13% and 86% are seen compared to the optimal passive system. This approach shows promise to provide a substantial increase in power capture for a minimal additional device cost and therefore a significant improvement in cost of energy would likely result. Areas for future study include methods of avoiding PTO tethers becoming slack and the imposition of a two-quadrant restriction on PTO operation.

References

[1] J. Falnes. A review of wave-energy extraction. *Marine Structures*, 20:185–201, 2007.

[2] A. Babarit, G. Duclos, and A.H. Clément. Comparison of latching control strategies for a heaving wave energy device in random sea. *Applied Ocean Research*, 26(5):227–238, 2005.

[3] A.F.O. Falcão. Modelling and control of oscillating-body wave energy converters with hydraulic power take-off and gas accumulator. *Ocean Engineering*, 24:2021–2032, 2007.

[4] A.F.O. Falcão. Phase control through load control of oscillating-body wave energy converters with hydraulic PTO system. *Ocean Engineering*, 35:358–366, 2008.

[5] J.A.M. Cretel, G. Lightbody, G.P. Thomas, and A.W. Lewis. Maximisation of energy capture by a wave-energy point absorber using model predictive control. In *Proceedings of the 18th IFAC World Congress*, volume 44, pages 3714 – 3721, Milan, Italy, 2011.

[6] J. Hals, J. Falnes, and T. Moan. Constrained optimal control of a heaving buoy wave-energy converter. *Journal of Offshore Mechanics and Arctic Engineering*, 133(1):011401–011401, 2010.

[7] G. Bacelli, J.V. Ringwood, and J-C. Gilloteaux. A control system for a self-reacting point absorber wave energy converter subject to constraints. In *Proceedings of the 18th IFAC World Congress*, volume 44, pages 11387 – 11392, Milian, Italy, 2011.

[8] M. Richter, M. E. Magana, O. Sawodny, and T. K. A. Brekken. Nonlinear model predictive control of a point absorber wave energy converter. *IEEE Transactions on Sustainable Energy*, 4(1):118–126, 2013.

[9] F. Fusco and J. V. Ringwood. A simple and effective real-time controller for wave energy converters. *IEEE Transactions on Sustainable Energy*, 4(1):21–30, 2013.

[10] A.J. Hillis, N.P. Sell, D.R.S. Chandel, and A.R. Plummer. Control of the CCell oscillating surge wave energy converter. *IFAC-PapersOnLine*, 50(1):14686 – 14691, 2017. 20th IFAC World Congress, Toulouse, France.

[11] A.J. Hillis, J. Roesner, N.P. Sell, D.R.S. Chandel, and A.R. Plummer. Investigation of the benefits of adaptive control applied to the nonlinear CCell wave energy converter. In *Proceedings of the Twelfth European Wave and Tidal Energy Conference*, Cork, Ireland, 2017.

[12] N. Sergiienko, B. Cazzolato, P. Hardy, B. Ding, and M. Arjomandi. Internal-model-based velocity tracking control of a submerged three-tether wave energy converter. In *Proceedings of the Twelfth European Wave and Tidal Energy Conference*, Cork, Ireland, 2017.

[13] W. E. Cummins. The Impulse Response Function and Ship Motions. *Schiffstechnik*, 9:101–109, 1962.

[14] A. Babarit and G. Delhommeau. Theoretical and numerical aspects of the open source BEM solver NEMOH. In *Proceedings of the 11th European Wave and Tidal Energy Conference*, Nantes, France, 2015.

[15] J.T. Scruggs, S.M. Lattanzio, A.A. Taflanidis, and I.L. Cassidy. Optimal causal control of a wave energy converter in a random sea. *Applied Ocean Research*, 42:1 – 15, 2013.

[16] G. Vissio, D. Valério, G. Bracco, P. Beirão, N. Pozzi, and G. Mattiazzo. Iswec linear quadratic regulator oscillating control. *Renewable Energy*, 103:372 – 382, 2017.

[17] N.Y. Sergiienko, A. Rafiee, B.S. Cazzolato, B. Ding, and M. Arjomandi. Feasibility study of the three-tether axisymmetric wave energy converter. *Ocean Engineering*, 150:221 – 233, 2018.